# $^{19}F$ and $^{13}C$ NMR Signal Assignment and Analysis in a Perfluorinated Ionomer (Nafion) by Two-Dimensional Solid-State NMR

**Q. Chen and K. Schmidt-Rohr***

*Ames Laboratory and Department of Chemistry, Iowa State University, Ames, Iowa 50011*

*Received February 4, 2004; Revised Manuscript Received May 25, 2004*

ABSTRACT: The $^{19}F$ and $^{13}C$ NMR resonances of the perfluorinated ionomer, Nafion, are assigned to their corresponding chemical groups using two-dimensional (2D) $^{13}C-^{19}F$ heteronuclear correlation and $^{19}F$-exchange NMR experiments under 28 or 30 kHz magic-angle spinning, combined with peak area and relaxation time information. On the basis of these new experimental data, we revise the assignment of more than half of the resolved $^{19}F$ NMR peaks. In particular, the backbone CF group is shown to resonate at −138 ppm, the side-group CF at −144 ppm, and the $SCF_2$ group, which can be selected by a $T_2$ filter, at −117 ppm. The $OCF_2$ groups resonate slightly downfield from the $CF_3$ fluorines. Deconvolution of the $^{19}F$ and $^{13}C$ spectra based on cross sections from the 2D spectra provides the peak widths and positions of all side group and several backbone sites. The inhomogeneous broadening observed in both $^{13}C$ and $^{19}F$ NMR spectra for the sites near the backbone CF group reveals static disorder near the branch point, which contrasts with the high conformational order of the rest of the backbone and the mobility of the ends of the side group.

## Introduction

Nafion is a solvent-resistant perfluorinated ionomer (see chemical structure in Figure 1a) with excellent proton conductivity that is used in chlor-alkali electrolysis, electrochemical devices, and $H_2/O_2$ fuel cells.[1−3] Despite Nafion's technological importance, its phase structure is not well understood.[3−6] $^{19}F$ NMR[7−12] provides excellent opportunities of characterizing segmental dynamics, chain packing, and domain sizes in Nafion with good sensitivity.[13−15] It relies crucially on the resolution of different $^{19}F$ NMR signals (see Figure 1b). The correct interpretation of the spectra in turn requires correct assignment of the signals to specific chemical sites in the repeat unit. We have found that the traditional assignment proposed for Nafion[16] and used in previous NMR studies of the phase structure and dynamics[15] is incorrect for several of the $^{19}F$ NMR peaks.

In this paper, we will present a well-founded $^{19}F$ NMR assignment based on fast-MAS $^{19}F$ peak areas, two-dimensional $^{13}C-^{19}F$ correlation NMR, two-dimensional $^{19}F$ spin-exchange NMR, and transverse-relaxation time ($T_2$) selection. In the interpretation of the $^{13}C-^{19}F$ correlation data, we use the $^{13}C$ NMR peak assignment obtained in our previous $^{13}C-^{19}F$ spectral editing experiments.[17] The widths of the $^{19}F$ and $^{13}C$ signals of nine specific sites are obtained from the 1D and 2D spectra and provide insights into the conformational order and dynamics of these sites.

## Experimental Section

**Sample.** The Dupont Nafion 117 ionomer was purchased in the form of a commercial fuel-cell-quality Nafion film, in the protonated form. The structure of the polymer is shown in Figure 1a. The ionomer has an equivalent weight of 1100, which corresponds to 14 $CF_2$ groups between branch points, on average. At this relatively high comonomer level, wide-angle X-ray crystallinity is negligible.[3] The membrane was kept in a desiccator and tightly rolled into a cylinder that fits snugly into the 2.5 mm rotor. Nevertheless, $^1H$ NMR shows that the sample had absorbed some water from the atmosphere. The effects of absorbed water on the side-group dynamics are currently under investigation in our laboratory.

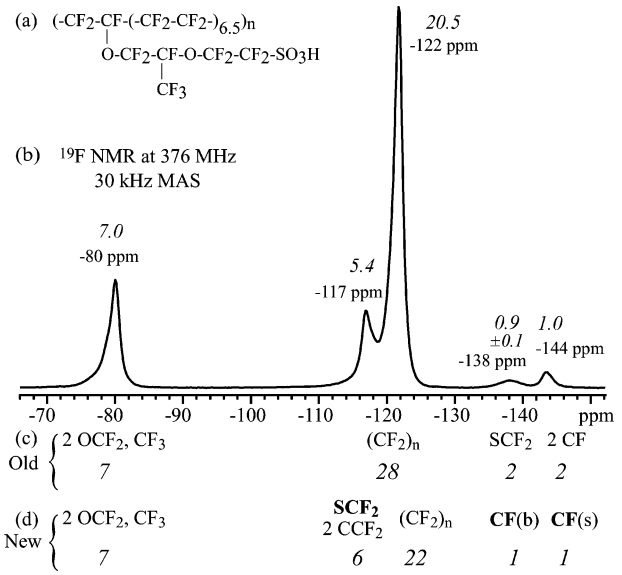


**Figure 1.** (a) Chemical structure of the Nafion ionomer. (b) $^{19}F$ NMR spectrum at a magic-angle spinning frequency of 30 kHz. Numerical values of peak integrals, including spinning sidebands (not shown), are shown in italics. (c) Traditional assignment with the predicted peak areas in italics. (d) Our revised assignment with predicted peak areas.

**NMR.** All the NMR experiments were performed at 100 MHz for $^{13}C$ and 376 MHz for $^{19}F$ on a Bruker DSX-400 spectrometer. All the spectra were acquired on the sample packed in a 2.5 mm rotor with Vespel end-caps, in a 2.5 mm X-H/F double-resonance magic-angle spinning (MAS) probehead at spinning frequencies $\nu_r$ of 28 or 30 kHz.

$^{19}F$ NMR spectra were acquired with a recycle delay of 3 s and a dwell time of 4 $\mu$s at $\nu_r = 30$ kHz after a pulse sequence of $t_r-\pi-$pulse$-t_r$, which produces a rotation-synchronized

* To whom correspondence should be addressed: Tel 515-294-6105; Fax 515-294-0105; e-mail srohr@iastate.edu.

10.1021/ma049759b CCC: $27.50 
Published on Web 07/09/2004

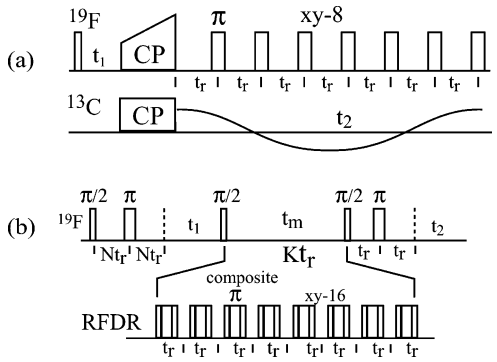


**Figure 2.** Two-dimensional NMR pulse sequences used in this work. (a) $^{19}F-^{13}C$ correlation at 28 kHz MAS with ramped cross-polarization and pulsed $^{19}F$ decoupling during $^{13}C$ detection.[17] (b) $^{19}F-^{19}F$ isotropic-shift exchange NMR at 30 kHz MAS. Before the evolution and detection period, the chemical shift is refocused in a Hahn spin echo. By increasing the duration of the first Hahn echo sequence, we can obtain a $^{19}F$ $T_2$-filtered 2D spectrum. During the mixing time $t_m$, one composite $\pi$-pulse per rotation period is applied in order to recouple the $^{19}F-^{19}F$ dipolar couplings (radio-frequency-driven recoupling, RFDR[18,19]).

Hahn spin echo. This avoids probehead deadtime effects and yields spectra without significant baseline distortion. Effects of differential $T_2$ relaxation during the Hahn-echo delays were <1%. The $^{19}F$ 90° pulse length was 2.5 $\mu$s, and the acquisition time was 8.2 ms. The $^{19}F$ signal of Teflon at −122 ppm was used as a secondary external reference. The peak positions quoted in ref 15 differ by ±2 ppm from those measured here. However, the positions read directly from the spectrum in Figure 2 of ref 15 are consistent with our results within ±1 ppm.

$^{19}F-^{19}F$ exchange spectra were acquired with the pulse sequence of Figure 2b. Radio-frequency dipolar recoupling (RFDR) of $^{19}F-^{19}F$ dipolar interactions by one composite $\pi$ pulse per rotation period was applied during the mixing time[18,19] in order to speed up $^{19}F$ spin diffusion and make it less dependent on the peak position.[20,21] The composite pulses $\pi/2_{\alpha+\pi}$ $\pi_\alpha$ $\pi/2_{\alpha+\pi}$ make the method less sensitive to the exact pulse flip angle. The phase α was incremented according to the *xy*-16 phase sequence (*xyxy yxyx* −*x*−*y*−*x*−*y* −*y*−*x*−*y*−*x*). The number of increments in $t_1$ was 100, with a $t_1$ dwell time of $t_r/2 = 16.67$ $\mu$s, which gives a wide enough spectral width in $\omega_1$ to avoid aliasing of the wings of any peaks. After the regular 2D processing, the spectra were postprocessed to avoid dispersive sidebands by adding the top quarter of the spectrum to the second quarter from the bottom and the bottom quarter to the second quarter from the top. The two central quarters are displayed, corresponding to a spectral width of $\omega_r$ and thus to a sideband-free $\omega_1$ dimension. A few spectra were acquired with a strong $^{19}F$ $T_2$ filter of 200 $t_r = 6.67$ ms duration applied before the evolution period in order to select the signal of the most mobile segments. The regular 2D experiments required 2.7 h each and the $^{19}F-^{19}F$ exchange spectra with $T_2$ filter 21 h each.

The $^{13}C-^{19}F$ correlation spectra were acquired with a CP contact time of 1.5 ms with a linear ramp on $^{19}F$ from 80% to 100% at a spinning frequency of 28 kHz. The number of increments in $t_1$ was 32 in a low-resolution, high-sensitivity experiment and 80 in a high-resolution experiment, with a $t_1$ dwell time of $t_r/2 = 17.86$ $\mu$s. Both cosine and sine data sets were recorded for each $t_1$ increment. The $^{19}F$ and $^{13}C$ 90° pulse lengths were 3.1 and 2.75 $\mu$s, respectively, and the acquisition time was 20.5 ms. The recycle delay was 2 s, and the experiments took 23 h each. Pulse sequences for the 2D experiments are shown in Figure 2.

For experiment-based deconvolutions of the one-dimensional $^{19}F$ and $^{13}C$ spectra, the MestRe-C software[22] was used. It permits input of experimentally determined information on peak positions, widths, and heights (integrals).

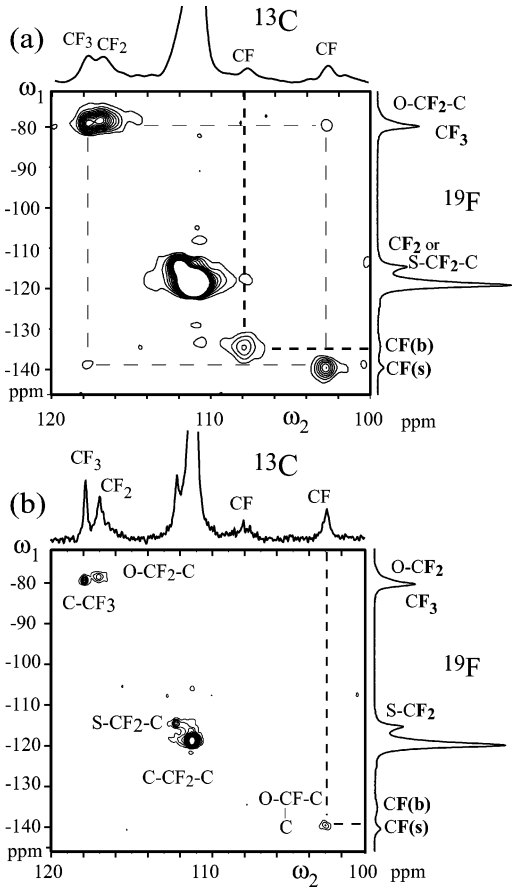


**Figure 3.** (a) $^{13}C-^{19}F$ heteronuclear correlation spectrum obtained with the sequence of Figure 2a at 28 kHz MAS, with acquisition and processing optimized for detection of low broad peaks, at the expense of signal resolution. The one-dimensional spectrum shown on the right is the regular $^{19}F$ NMR spectrum. (b) Same as in (a), but from a different data set measured with full resolution. In the $^{13}C$ spectra at the top of the spectra, assignments to $CF_n$ groups as previously obtained by us[17] are indicated.

## Results and Discussion

Figure 1b displays the experimental peak integrals for the $^{19}F$ NMR spectrum, with the integral of the rightmost peak set to 1.0. The traditional assignment,[15,16] obtained originally from spectra that were not sufficiently resolved to permit reliable peak integration, is indicated in Figure 1c, together with the corresponding peak areas in the third row. The new assignment proposed in this paper is shown in Figure 1d. The resulting peak integrals agree quite well with the experimental values. In the following, we will present the experiments from which this new assignment was derived, using the pulse sequences shown in Figure 2.

**$CF_3$ and CF Signal Assignment.** We can assign several of the $^{19}F$ NMR resonances through correlation of the $^{19}F$ peaks with the signals of $^{13}C$ sites to which they are bonded, using the $^{19}F-^{13}C$ pulse sequence of Figure 2a. We have shown that the $^{13}C$ spectrum contains one more resolved signal than the $^{19}F$ spectrum and that it is quite amenable to spectral editing. As indicated in Figure 3a, the number of fluorines bonded to a given carbon was previously determined by us[17] using the fluorine equivalent of the attached proton test.[23] In particular, this distinguishes CF groups unambiguously from $CF_2$ moieties. Using the $^{19}F-^{13}C$ correlation spectra of Figure 3, these assignments can

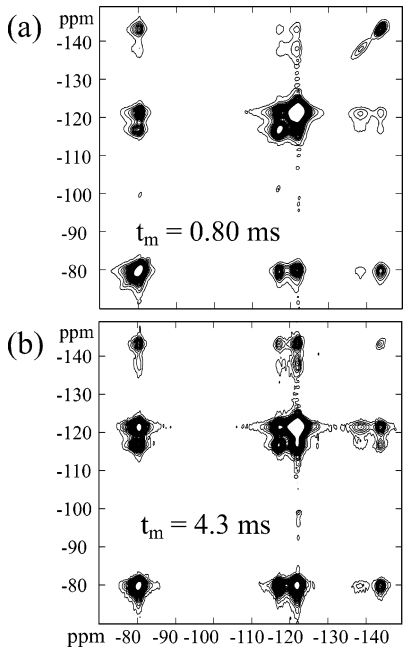


**Figure 4.** Representative two-dimensional $^{19}$F exchange NMR spectra at $\nu_r = 30$ kHz with RFDR pulses during the mixing time, using the pulse sequence of Figure 2b. Mixing times: (a) 0.80 ms; (b) 4.3 ms. Forty contour lines from 0.15% to 6% of the maximum intensity are plotted.

be converted into $^{19}$F assignments in terms of $CF_3$, $CF_2$, and CF groups. Note in particular that a broad peak in Figure 3a clearly correlates the CF signal at 108 ppm in the $^{13}$C dimension with the −138-ppm peak in the $^{19}$F spectrum, which was previously assigned to a $CF_2$ group,[15,16] which is now seen to be incorrect.

Figure 4 exhibits contour plots of 2D exchange $^{19}$F NMR spectra of Nafion, taken at a spinning frequency of 30 kHz with the pulse sequence of Figure 2b. In particular, radio-frequency driven recoupling (RFDR) by one composite $\pi$-pulse per rotation period[18,19] was applied during the mixing time $t_m$ to speed up the $^{19}$F spin exchange. The two spectra shown are representative of a series of 2D spectra obtained with 11 mixing times between 0.133 and 8.5 ms. Cross sections at the positions of the peaks in $\omega_1$ are presented in Figure 5 for three mixing times. The cross-peaks show the proximities of the various $^{19}$F sites. Cross-peaks between fluorines in neighboring segments will be particularly strong. Nevertheless, cross-peaks are also observed between more distant segments. These could arise from direct through-space contacts or multiple transfer steps ($^{19}$F spin diffusion). We believe that for $t_m < 1$ ms they mostly represent direct through-space contacts: at the short mixing times, all cross-peaks are small and indirect transfer peaks should be small of second order.

The cross-peaks observed in Figure 4 enable us to assign the two CF signals at −138 and −144 ppm to the backbone and side group, respectively. The strong cross-peaks between the side-group peak at −80 ppm and the OCF signal at −144 ppm, seen both in the contour plots of Figure 4 and in the cross sections of Figure 5a,e, show that the latter is part of the side group. Conversely, the cross-peak between the backbone signals at −117 and −122 ppm and the −138 ppm of CF signal is more intense (in terms of integrated intensity) than that of the other CF peak (see Figures 4 and 5b,d), assigning the downfield (i.e., left) CF peak to the branch point in the backbone.

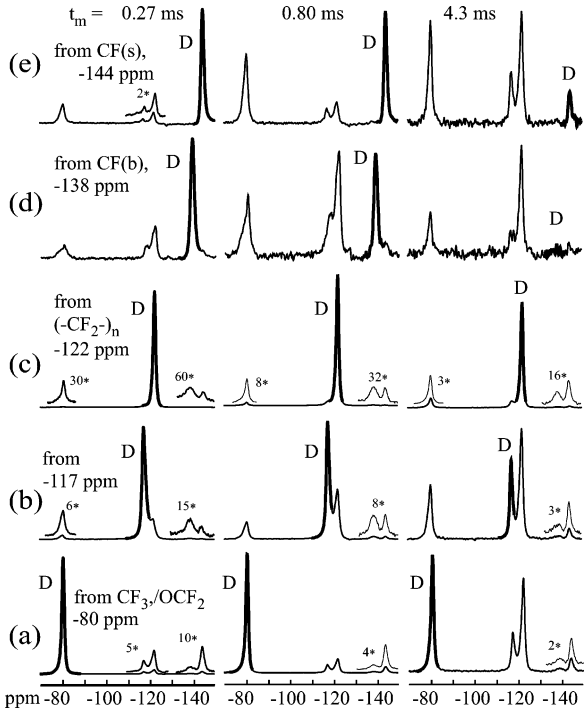


**Figure 5.** One-dimensional cross sections from 2D $^{19}$F exchange spectra as shown in Figure 4, with mixing times of 0.27 ms (left column), 0.80 ms (center column), and 4.3 ms (right column). The $\omega_1$ positions of the cross sections (a−e) are indicated. Diagonal peaks are labeled by "D" and a thicker line. Peak widths and relative intensities are more easily recognizable here than in the contour plots of Figure 4.

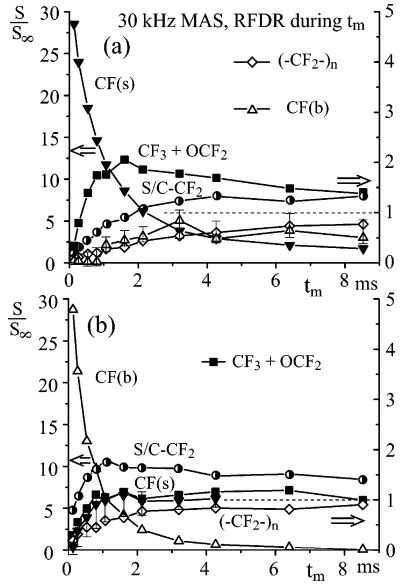


**Figure 6.** Mixing time dependence of CF-group cross-peak intensities in series of two-dimensional $^{19}$F exchange NMR spectra acquired at 30 kHz (for examples see Figures 4 and 5). (a) Peak areas in the cross section at −144 ppm; (b) peak areas in the cross section at −138 ppm. The plots show the fraction of the peak area in cross sections as shown in Figure 5, divided by the fractional area in the 1D spectrum without selection. Thus, the value reached after full equilibration is unity for each peak. Full symbols: side group; open symbols: backbone sites.

To enable a more quantitative analysis of the exchange processes, Figure 6 shows the $t_m$ dependence of the integrated peak intensities in the cross sections at $\omega_1 = -144$ and −138 ppm. The long-time intensity of each peak is normalized to unity. This is achieved by

dividing the fraction of the area of a given peak in a given cross section by the fractional area of that peak in the 1D spectrum without selection. This normalization corresponds to the magnetization per fluorine at a given mixing time, if the final magnetization per fluorine is equal to unity. The −144 ppm peak is seen to transfer its magnetization most quickly to side-group fluorines, while the −138 ppm peak shows faster spin diffusion to fluorines in the backbone. This proves the location of the CF moieties in the side group and backbone, respectively.

Confirmation of this assignment is also found in the $^{13}C-^{19}F$ spectrum in Figure 3a, which contains indications of two weak cross-peaks, near the upper right and lower left corners of the spectrum, between the upfield OCF signal and the $CF_3$ fluorine signal, which again identify the peak at −144 ppm as the side group OCF.

**$OCF_2$ Peak Assignment.** Next, we need to determine the assignment of the $CF_2$ resonances. The repeat unit contains two $OCF_2$ groups and one $SCF_2$ moiety. Two of these resonate near 117 ppm in the $^{13}C$ spectrum and near −80 ppm in the $^{19}F$ spectrum, according to the $^{19}F-^{13}C$ HETCOR spectra of Figure 3, the attached-fluorine test in ref 17, and the $^{13}C$ and $^{19}F$ peak integrals. Their similar, downfield chemical shifts in both $^{19}F$ and $^{13}C$ spectra indicate that these two are the two $OCF_2$ groups. This is in agreement with the previous assignment.[15,16] The line shape of the band near 117 ppm in the $^{13}C$ spectrum indicates a superposition of a broad and a narrow band; we assign the narrower peak to the $OCF_2$ near the end of the side group and the broader to the $OCF_2$ near the branch point (see below). Note that the HETCOR spectrum separates these $OCF_2$ signals from the $CF_3$ resonance, which permits the position of the narrower $OCF_2$ resonance to be determined more accurately than from the 1D $^{19}F$ NMR spectrum.

**$SCF_2$ Peak Assignment.** Where is the signal of the $SCF_2$ segment? According to the electronegativities of sulfur, carbon, and oxygen (2.5, 2.5, and 3.5, respectively), we should look for the $SCF_2$ resonance between the $OCF_2$ and the $CCF_2$ signals in both the $^{19}F$ and the $^{13}C$ spectrum and most likely closer to the $CCF_2$ signal. Indeed, the HETCOR spectrum of Figure 3b shows a distinct, sharp peak at −117 ppm ($^{19}F$) and 112 ppm ($^{13}C$), with a shape and intensity very similar to that of the $CF_3$ resonance. We will show in the following that this must be the $SCF_2$ signal.

The −117-ppm signal of the $^{19}F$ spectrum has traditionally been assigned to the four fluorines of the backbone $CF_2$ groups next to the OCF branch point.[15,16] We concur with this assignment but note that the peak's integral corresponds to 5.4 fluorines (see Figure 1), indicating that another $CF_2$ group contributes to this signal. Potentially, this could be due to one "amorphous" $CF_2$ group per repeat unit, as was suggested in ref 15. However, with such an assignment the $SCF_2$ signal would still be missing.

To provide a positive proof that this is the $SCF_2$ signal, we show that this site is close to an $OCF_2$ segment, while not being in close spin-diffusion contact with the backbone sites at −122 ppm. To remove the overlapping signals of the backbone $CF_2$ groups next to the CF branch point, we select the $SCF_2$ signal by a $^{19}F$ transverse relaxation time ($T_2$) filter. The $T_2$ relaxation time of the $SCF_2$ fluorines is expected to be relatively long for two reasons: (i) mobility of the end of the side groups can be expected to be high, and (ii) the fluorine density near this group is lower than near the other $CF_2$ groups, given that it is flanked by the fluorine-less $SO_3$ and a single $OCF_2$ group. Figure 7a shows the $T_2$-filtered $^{19}F$ spectrum of Nafion, which retains signals at −80, −117, and −122 ppm. These are assigned to $CF_3$, $SCF_2$, and some backbone $CF_2$ groups, respectively. The surprisingly long $T_2$ of some of the backbone $CF_2$ groups, at −122 ppm, will be discussed in a future publication.

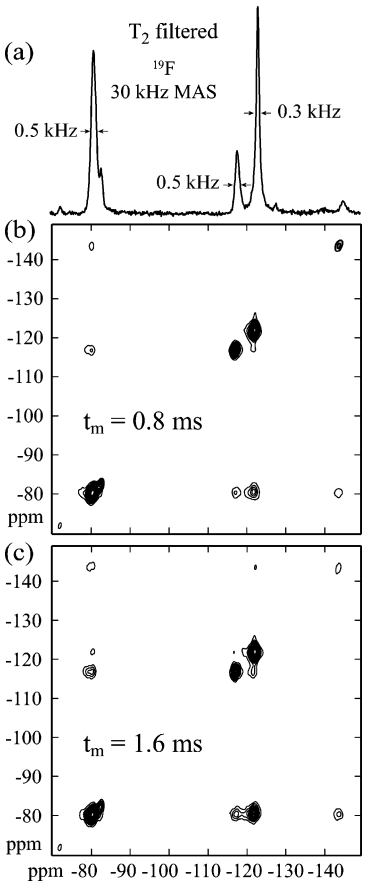


**Figure 7.** (a) One-dimensional $T_2$-filtered $^{19}F$ spectrum with $2N = 200$ rotation periods of total filter time (6.67 ms). The signals of the most mobile segments are selected. (b, c) Two-dimensional $^{19}F$ exchange NMR spectra after a $2\tau = 6.67$ ms $^{19}F$ $T_2$ filter before the evolution period ($2N = 200$ rotation periods in the pulse sequence of Figure 2b). During the mixing time, RFDR homonuclear recoupling was applied. Note that due to the $T_2$ selection in $\omega_1$, the 2D spectra are expected to be asymmetric. Forty contour lines from 2% to 80% of the maximum intensity are plotted.

The same $T_2$ selection was applied in the first dimension of a $^{19}F$ 2D exchange experiment with RFDR homonuclear recoupling. Thus, a cross section at $\omega_1 = -117$ ppm shows cross-peaks only of segments in dipolar or spin-diffusion contact with the mobile $CF_2$ group resonating at −117 ppm (which we will show to be the $SCF_2$ group). The largest cross-peak is observed at ca. −80 ppm (see Figure 8a,b). Its 1.0 kHz width is clearly larger than that of the $CF_3$ signal (0.6 kHz), proving that this is predominantly an $OCF_2$ signal. No significant cross-peaks to the CF signals are observed. Thus, we have shown that the long-$T_2$ $CF_2$ group is near an $OCF_2$ group and not close to the branch point or side-group CF sites.

The cross sections of Figure 8b also exhibit significant cross-peaks from the $SCF_2$ to the backbone fluorines.

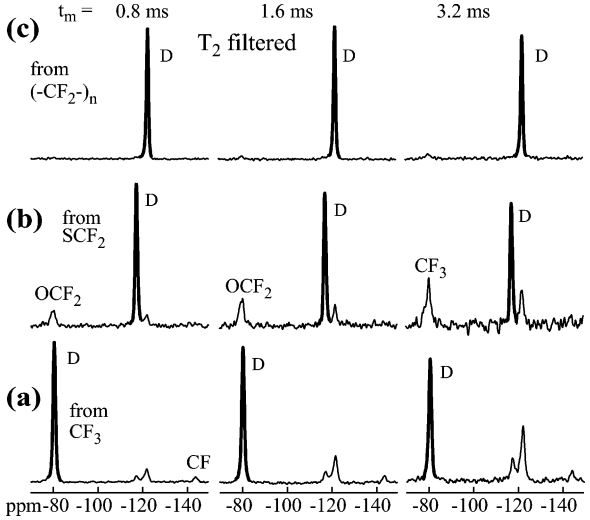


**Figure 8.** Cross sections from three $T_2$-filtered $^{19}$F 2D exchange spectra, taken at the three long-$T_2$ peaks in $\omega_1$ as indicated (a−c). Mixing times: 0.80 ms (left column), 1.6 ms (center column), and 3.2 ms (right column).

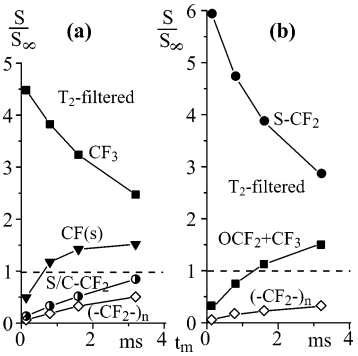


**Figure 9.** Mixing time dependence of cross-peak intensities in series of $T_2$-filtered two-dimensional $^{19}$F exchange NMR spectra acquired at 30 kHz (for examples see Figures 7 and 8). (a) Peak areas in the cross section at −80 ppm; (b) peak areas in the cross section at −117 ppm. The plots show the fraction of the peak area in cross sections as shown in Figure 8, divided by the fractional area in the 1D spectrum without selection. Full symbols: side group; open symbols: backbone sites.

However, this does not indicate particularly close proximity of the $T_2$-selected $CF_2$ groups to the backbone. The intensity of this peak, relative to the large equilibrium value, is actually quite small. Otherwise put, the cross-peak between a small signal and a large signal, like the backbone $CF_2$, will be quite large due to the large number of backbone $CF_2$ sites contributing to the peak, even if each individual transfer rate is small. This is confirmed by observing that the $CF_3$ cross sections of Figure 8c show similarly large cross-peaks to the backbone $CF_2$.

Plots of the cross-peak intensity as a function of the mixing time (Figures 9 and 10) show the spin-exchange dynamics quantitatively. They display the mixing-time dependence of the diagonal and cross-peaks, with the long-time intensity of each peak normalized to unity as described above. Figure 9 shows the data obtained after the $T_2$ filter and Figure 10 the corresponding unfiltered data (from 2D spectra as shown in Figure 4) for reference. Spin diffusion from the −80 ppm side-group fluorines (Figures 9b and 10b) shows fast transfer to other side-group sites and only slow transfer to the backbone. Similarly, the $SCF_2$ magnetization in Figure

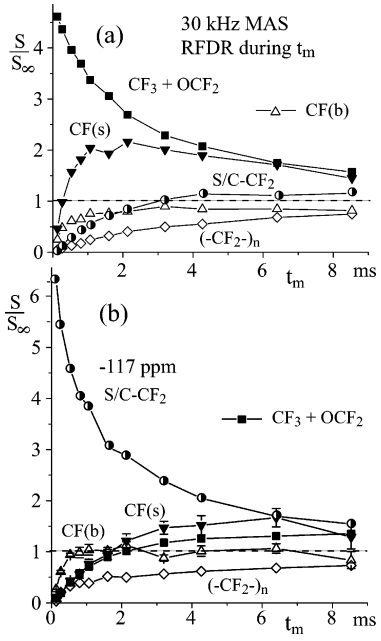


**Figure 10.** Mixing time dependence of cross-peak intensities in series of (unfiltered) two-dimensional $^{19}$F exchange NMR spectra acquired at 30 kHz with RFDR recoupling (examples are shown in Figures 4 and 5). (a) Peak areas in the cross section at −80 ppm; (b) peak areas in the cross section at −117 ppm. Normalization and symbols are the same as in Figure 9.

9b is seen to transfer most quickly to side-group fluorines, confirming that the −117 ppm, long-$T_2$ $CF_2$ groups are indeed located in the side group. In contrast, the spin diffusion from the unfiltered −117 ppm peak (Figure 10b), which contains a majority of backbone fluorines, occurs most quickly to backbone sites. Another example of spin diffusion from the backbone is shown in Figure 6b for the CF branch point.

Close inspection of the curves in Figures 9, 10, and 6 shows slower transfer rates from the $SCF_2$ than from the other sites; we attribute this to motional averaging of F−F dipolar couplings in the mobile end of the side group. The $T_2$-filtered −117 ppm fluorine shows the slowest transfer to the backbone $(-CF_2-)_n$ among all the data shown in Figures 6, 9, and 10, confirming its position near the end of the side group.

**Comparison with Previous Assignments.** Previous $^{19}$F NMR assignments were based on comparisons with a small number of model compounds.[16] Peak resolution in this early solution NMR study was insufficient to provide accurate peak integrals. When higher fields had become available, the inconsistent area of the −117 ppm peak was explained in terms of an amorphous-backbone contribution.[15] Nevertheless, the factor-of-2 inconsistency between peak areas in the previous assignment and the experimental integrals of the $CF_3$ plus $OCF_2$ peak at ca. −80 ppm relative to the signals at −138 and −144 ppm is striking (see Figure 1). Our assignments of the two latter signals to the CF groups are unambiguous, being supported both by clear cross-peaks in the HETCOR spectrum of Figure 3a and by the peak integrals. Our detection of a side-group ($SCF_2$) peak at −117 ppm where only backbone signals had been assigned changes the interpretation of the amorphous−crystalline phase structure proposed in ref 15. Generally, we note that all the resonance positions in the $^{13}$C spectrum of Nafion follow the trend expected based on the electronegativity of the three substituents

**Table 1. Parameters of the Experiment-Based Deconvolution of the $^{19}F$ and $^{13}C$ NMR Spectra of Nafion: (a) $^{19}F$ NMR Peaks; (b) $^{13}C$ NMR Peaks[a]**

| (a) $^{19}F$ | $CF_3$ | $OCF_2$ | $SCF_2$ | | $(CF_2)_n$ | | | | | CF(b) | CF(s) |
|---|---|---|---|---|---|---|---|---|---|---|---|
| rel intensity | 3 | 2 | 2 | 2 | 4 | 4 | 4 | 4 | 8 | 1 | 1 |
| position (ppm) | −80.4 | −80.1 | −79.9 | −117.1 | −118.2 | −121.4 | −121.4 | −121.9 | −122.1 | −138.4 | −143.8 |
| width (kHz) | 0.46 ± 0.03 | 2.06 ± 0.2 | 0.95 ± 0.09 | 0.54 ± 0.05 | 1.3 ± 0.2 | 1.2 ± 0.2 | 0.8 ± 0.2 | 0.7 ± 0.1 | 0.40 ± 0.08 | 1.5 ± 0.1 | 0.77 ± 0.03 |
| Lor/Gauss | 0.8 | 0 | 0 | 0.2 | 1.0 | 0.4 | 0.4 | 0.0 | 0.7 | 0.7 | 0.4 |
| (b) $^{13}C$ | | | | | | | | | | | |
| rel intensity | 1 | 1 | 1 | 1 | 2 | 2 | 2 | 4 | 4 | 1 | 1 |
| position (ppm) | 117.90 | 116.73 | 117.02 | 112.24 | 111.79 | 111.41 | 111.26 | 111.25 | 111.25 | 108.10 | 102.94 |
| width (ppm) | 0.26 ± 0.03 | 1.1 ± 0.2 | 0.50 ± 0.06 | 0.37 ± 0.06 | 1.35 ± 0.3 | 0.9 ± 0.1 | 0.6 ± 0.1 | 0.41 ± 0.08 | 0.26 ± 0.05 | 1.4 ± 0.2 | 0.49 ± 0.04 |
| Lor/Gauss | 1 | 0.5 | 0.8 | 0.6 | 1.0 | 0 | 1.0 | 0 | 0.4 | 0 | 1.0 |

[a] Lor:Gauss refers to the Lorentzian:Gaussian ratio in the peak shape.

of the carbon observed. The electronegativity also accounts for the similar trends in the $^{19}F$ spectrum. As a result, the positions of peaks in the 2D HETCOR spectra of Figure 3 follow a simple trend.

While the assignment of the peak near −80 ppm to $CF_3$ and $OCF_2$ groups has not changed, we have now been able to determine the relative $^{19}F$ NMR peak position of these unresolved signals and seen indications of inhomogeneous line broadening of the signal of the $OCF_2$ group nearest to the backbone.

**Widths of Resonances.** On the basis of a reliable peak assignment and the cross sections from the 2D $^{19}F$ exchange spectra, we can proceed to interpret the differences in signal line widths in terms of conformational disorder and dynamics. We can combine the peak-width information on both $^{19}F$ and $^{13}C$ NMR peaks, which strengthens the argument. Table 1a and Figure 11 summarize the information on Nafion $^{19}F$ peak positions, areas, and widths obtained from the various 2D spectra presented in this work.

A significant broadening of the backbone CF signal relative to the other peaks is observed in both the $^{19}F$ and $^{13}C$ NMR spectra; see Figures 1 and 3 (or Figures 11d and 12a). In the 2D spectrum of Figure 4a, this signal exhibits an extended peak shape along the diagonal, which proves that this resonance is inhomogeneously broadened. This indicates a distribution of local environments that do not interconvert on the NMR time scale (0.1 ms). While the broad peaks from sites near the branch point are not resolved in the standard 1D spectrum, the $^{19}F$ 2D exchange spectra provide convincing experimental evidence for their existence. To emphasize this, Figure 11a displays the spectrum of the sites near the branch point (Figure 5d at short mixing time) on the same scale as the regular 1D spectrum. Three broad resonances of sites near the branch point are observed selectively, without significant overlap from the otherwise dominant narrow resonances. Fluorine−fluorine *J*-couplings are <0.22 kHz (<0.6 ppm) and therefore do not contribute significantly to the observed line widths.

The −80 ppm peak in Figure 11a shows a bimodal shape, with a major 2.1 kHz wide and a minor narrow component. These are assigned to the $OCF_2$ and $CF_3$ groups, respectively. The large width of the $OCF_2$ signal indicates similar static conformational disorder as observed for the CF branch point itself. A hint of a corresponding inhomogeneously broadened $OCF_2$ signal is observed in the lower left corner of the 2D exchange spectrum of Figure 4, where a ridge along the diagonal is detectable. Similarly, the $^{13}C$ line width of the signal of one of the $OCF_2$ groups resonating near +116.5 ppm appears to be rather large in the $^{13}C$ spectrum at the top of Figure 3b.

It is interesting to observe that in Figure 5b,d the line width of the $^{19}F$ NMR cross-peak at −122 ppm (0.9−1.1 kHz) at short mixing times is clearly larger than that of the total −122 ppm peak in the 1D spectrum (0.6 kHz). Figure 11b,d provides a direct comparison of these signals. In spectra of Figure 5b,d the magnetization originates predominantly at or near the branch point. This indicates a larger degree of disorder—chemical or physical—among the $CF_2$ backbone groups near the branch point. Given that the signal at −117 ppm reflects two backbone $CF_2$ groups, the 1:2 area ratio of the broad peaks near −117 and −122 ppm in Figure 5d for $t_m = 0.8$ ms shows that the disorder affects at least four other $CF_2$ groups near the average branch point. In other words, the average branch point is flanked by at least three $CF_2$ groups on either side that are conformationally disordered.

Since the copolymerization of Nafion is random, we need to consider whether the line broadening of sites near the branch point can be attributed to "sequence effects", i.e., the proximity of another branch point to the one that we are observing. The statistical probability of a monomer units being branched is $1:(6.5 + 1) = 13\%$. To calculate the probability of finding another branch-point near the one observed in our spectra, we first consider a branched monomer unit and its two monomer neighbors. Each neighbor has a statistical probability of 13% of being branched, and the probability of two branched neighbors is $0.13^2 = 2\%$. Thus, the probability of not having a branched neighbor within three bonds from the branch point on one side, and within two bonds on the other, is $100\% - 2 \cdot 13\% - 2\% = 72\%$. We obtain the simpler probability of not having a branched neighbor within three bonds from the branch point (on either side), which is 66%, by including half of another monomer unit on the "two-bond side" from the branch point (along the backbone), which has a probability of $13\%/2 = 6.5\%$ of containing a branch point.

The $OCF_2$ group is separated from the branch point by two bonds, and thus its probability of having another branch point five or more bonds away is 67%. Since significant chemical shift effects do not extend over five or more bonds, we conclude that for this group in particular, the significant line broadening of 1.1 and 5.5 ppm observed in $^{13}C$ and $^{19}F$ NMR, respectively, is not due to sequence effects.

For the $CF_2$ groups near the branch point, the statistical presence of nearby branch points is less than for the CF branch point itself, since that branch point permits close proximity of another branch point only on

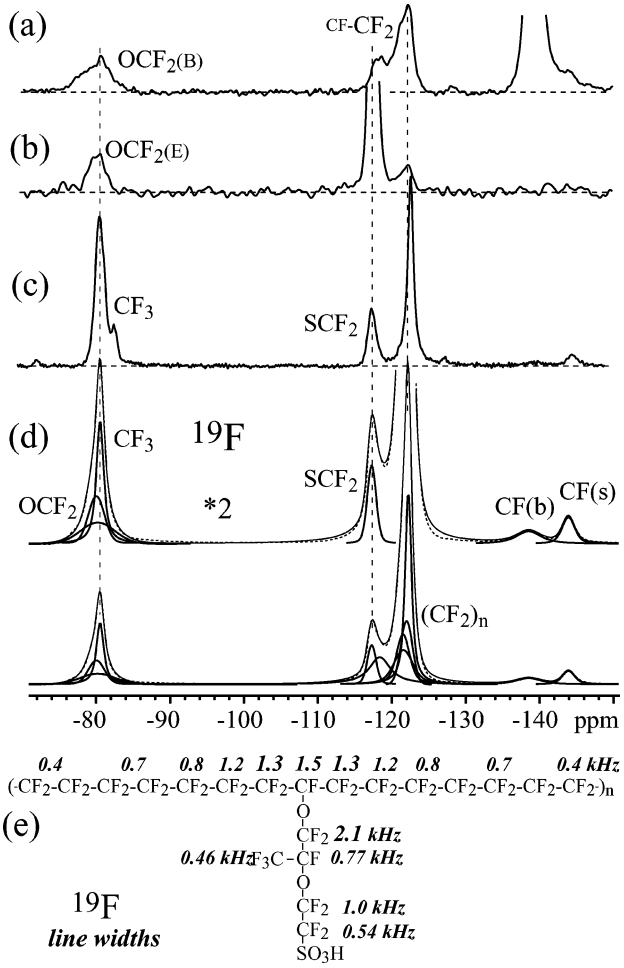


**Figure 11.** Deconvolution of the $^{19}$F NMR spectrum of Nafion based on peak positions and widths in cross sections from 2D spectra presented in this work. (a) Slice from a 2D exchange spectrum at the branch point CF resonance in $\omega_1$ (Figure 5d for $t_m$ = 0.27 ms). It clearly shows the broad resonances of sites near the branch point, including the neighboring $OCF_2$ group. The diagonal peak at −138 ppm, whose width is only a fraction of the full inhomogeneous width of that signal, has been clipped. (b) Slice from a $T_2$-filtered 2D exchange spectrum at the $SCF_2$ resonance in $\omega_1$ (Figure 8b for $t_m$ = 0.8 ms). It shows the resonance of the $OCF_2$ group near the end of the side group selectively. (c) $T_2$-filtered $^{19}$F NMR spectrum of Figure 7a, revealing the signals of sites nearest to the ends of the side group, and of the most ordered backbone sites. (d) Fit of the 1D $^{19}$F NMR spectrum of Nafion based on the peak positions and widths in (a−c). Dashed line: experimental spectrum. Top traces: two-folded vertically expanded plots, without backbone-$CF_2$ fit components. (e) Widths (full widths at half-maximum) of $^{19}$F NMR peaks at 30 kHz MAS for the various sites in Nafion. The line broadening in excess of 0.6 kHz has been shown to be inhomogeneous in nature. Therefore, the width of the broader peaks should be considered in ppm. To convert to ppm, multiply the given numbers by 2.66 ppm/kHz. Error margins are listed in Table 1a.

one side. The probability of another branch point being three or more bonds away from these $CF_2$ groups is 72%. $^{13}$C chemical shift simulations indicate that the dispersion of chemical shifts resulting from branch points that are three or more bonds away is small, <0.2 ppm, which is less than the smallest $^{13}$C line width observed here.

The peaks from the side group (CF, $CF_3$, and $SCF_2$) are quite narrow. The signal of the $OCF_2$ group near the end of the side group is observed selectively in the $SCF_2$ slice of a $T_2$-filtered 2D exchange spectrum (see Figure 7a or 11c), which displays sharp $CF_3$ and $SCF_2$ signals at −80 and −117 ppm, respectively. The reduced widths indicate that these segments are quite mobile, with fast exchange between the various possible conformations resulting in a similar average chemical shift for sites in different side groups. This conformational mobility is not consistent with a rigid structure up to the $CF_2$−S moiety, which was suggested in a recent simulation of the Nafion side group.[24] A more detailed experimental analysis of the mobility by means of anisotropic interactions, and the effect of water, will be presented in a later publication.

**Synopsis.** Figure 11d,e summarizes the information on Nafion $^{19}$F peak positions, areas, and widths obtained from the various 2D spectra presented in this work. In Figure 11d, the best fit of the $^{19}$F spectrum and its component peaks are shown and compared with the experimental spectrum (dotted line). Figure 11e and Table 1a present the widths of $^{19}$F resonances obtained from this analysis. The large inhomogeneous line widths for sites near the branch point, which are of the order of 1.5 kHz or 4 ppm, clearly reveal static disorder in that part of the structure, which is seen to extend from the branch point over two bonds in all three directions.

Figure 12 and Table 1b provide a similar analysis of the $^{13}$C peak positions and widths. A deconvolution of the $^{13}$C spectrum (Figure 12a) was performed on the basis of the known peak areas and on the cross sections from the HETCOR spectrum of Figure 3b, several of which are shown in Figure 12b. Figure 12c shows that, as with $^{19}$F signals, increased line widths are observed for sites near the branch point, including the neighboring $OCF_2$ group. Figure 13 shows a plot correlating the $^{19}$F and $^{13}$C line widths found, confirming the similar trends. It is interesting to note that the observed 4.2:1 ratio of the $^{19}$F and $^{13}$C ppm values, reflected in the slope of the best-fit straight line in Figure 13, closely matches the 63 ppm:15 ppm = 4.2:1 ratio of the ranges of the isotropic peak positions in the $^{19}$F and $^{13}$C spectra of Nafion.

The data in Table 1 indicate that the intensity of two $CF_2$ groups per repeat unit is missing from the $^{19}$F NMR $CF_2$ backbone resonance, while the intensity ratios expected on the basis of the ion-exchange capacity are observed in the $^{13}$C spectrum. The reason for the missing $^{19}$F NMR intensity is unclear. It is not due to spinning sidebands, which represent a minor signal fraction and were considered in the analysis. Possibly, certain backbone sites are in an intermediate motional regime where the large $^{19}$F CSA and dipolar coupling results in a very short $T_2$ relaxation time which broadens the signal beyond detectability.

The small width of the main $(-CF_2-)_n$ backbone resonance in both $^{19}$F and $^{13}$C NMR spectra (33 Hz in the latter), and the agreement with the peak position of PTFE, indicates that major portions of the backbone form conformationally ordered helices as found in PTFE. In contrast, the inhomogeneous broadening of $^{13}$C NMR backbone-$CH_2$ resonances in glassy polymers is several hundred hertz (e.g., polystyrene: $10^3$ Hz; poly(ethyl methacrylate): $3 \times 10^2$ Hz) due to the various conformational and packing environments. The related dynamics and packing of the Nafion backbone helices will be further elucidated in a subsequent paper.

**Implications for Segmental Dynamics.** As discussed above, the $^{19}$F and $^{13}$C line widths have revealed relatively static disorder near the branch site and mobility of the ends of the side groups. In previous

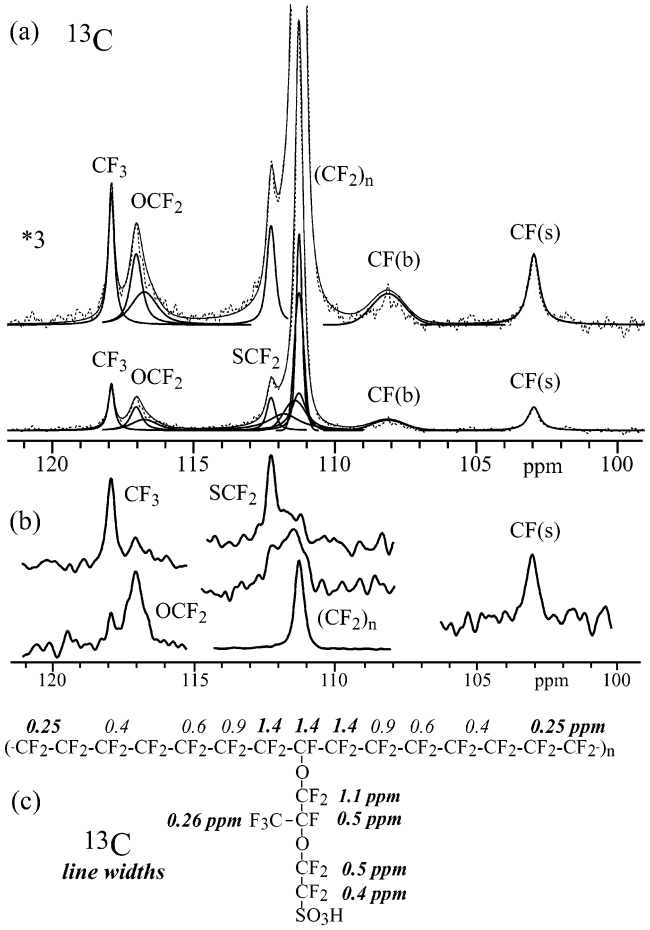


**Figure 12.** (a) Fit of the 1D $^{13}C$ NMR spectrum of Nafion, obtained under 28-kHz MAS and presented first in our previous publication[17] (dashed line), deconvoluted based on the peak assignments obtained in this work. For overlapping peaks, the deconvolution is based on the peak positions and widths extracted from the HETCOR spectrum of Figure 3b. Relevant parts of cross sections from that spectrum are shown in (b). (c) Widths (full widths at half-maximum) of $^{13}C$ NMR peaks at 28-kHz MAS for the various sites in Nafion as used in the fit in (a). Values assigned to specific sites with certainty are given in bold. Error margins are listed in Table 1b.

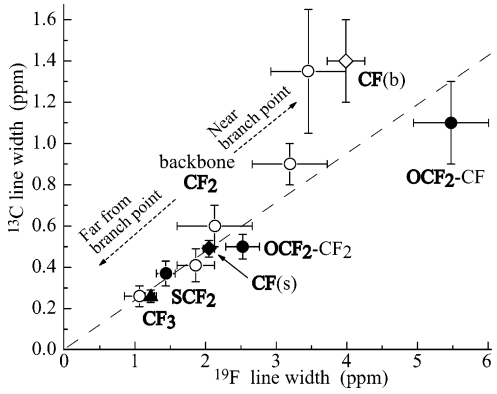


**Figure 13.** Correlation plot of $^{19}F$ and $^{13}C$ NMR line widths as listed in Table 1. Side-group sites are shown as filled symbols and backbone sites as open symbols. A best-fit straight line is shown as a guide to the eye.

investigations of Nafion, due to the incorrect assignment of the broad signal at −138 ppm and the failure to separate the true $SCF_2$ signal at −117 ppm, this conclusion could not be reached. Our data also indicate large-amplitude rotational dynamics of the $(-CF_2-)_n$ backbone, which will be proven and discussed in a future publication.

The corrected assignment means that some of the conclusions about backbone dynamics in relatively dry and in swollen Nafion as proposed in ref 15 should be revised. The signal of the mobile side group $SCF_2$ moiety at −117 ppm was incorrectly interpreted as amorphous $CF_2$ in the backbone. According to our study, no amorphous backbone $CF_2$ with nearly isotropic mobility is present in Nafion at ambient humidity.

## Conclusions

The $^{19}F$ and $^{13}C$ NMR signals of the perfluorinated ionomer, Nafion, have been assigned on the basis of various two-dimensional NMR spectra. In combination with our previous $^{13}C$ spectral editing based on one-bond $^{19}F-^{13}C$ *J*-couplings, the one-bond $^{19}F-^{13}C$ heteronuclear correlation clearly identifies the $^{19}F$ signals of the two CF groups in the repeat unit. The $^{19}F$ NMR backbone and side group CF sites are assigned unambiguously to the signals at −138 and −144 ppm, respectively, on the basis of cross-peaks in $^{19}F$ spin exchange spectra with RFDR recoupling during the mixing time. The $CF_3$ and $OCF_2$ signals, near −80.4 and −79.8 ppm, are clearly resolved in the $^{13}C$ dimension of the HETCOR spectrum. On the basis of its high mobility, the $SCF_2$ site near the end of the side group is selected by means of a $^{19}F$ $T_2$ filter, and its identity is confirmed by its proximity to the more mobile of the two $OCF_2$ groups. Cross sections from the 2D spectra, combined with $T_2$ filtering, provide the $^{19}F$ and $^{13}C$ peak positions and widths of all side group and several backbone sites. These data are confirmed and refined by fits of the 1D $^{19}F$ and $^{13}C$ NMR spectra. Relatively static disorder near the branch point and increased mobility near the ends of the side group is revealed by the differential line broadening of the $^{19}F$ and $^{13}C$ NMR signals. The position and small width of the peak of the backbone $CF_2$ groups in both the $^{13}C$ and the $^{19}F$ spectrum indicate straight, PTFE-like helices between the branch points.

**Acknowledgment.** This work was supported by the Director for Energy Research, Office of Basic Energy Science, in the Materials Chemistry Program of Ames Laboratory, operated for the U.S. Department of Energy by Iowa State University (Contract W-7405-Eng-82).

## References and Notes

(1) Yeo, R. S. *ACS Symp. Ser.* **1982**, *No. 180*, 453.
(2) Bergner, D. *J. Appl. Electrochem.* **1982**, *12*, 631.
(3) Gierke, T. D.; Munn, G. E.; Wilson, F. C. *J. Polym. Sci., Polym. Phys. Ed.* **1981**, *19*, 1687.
(4) Yeo, S. C.; Eisenberg, A. *J. Appl. Polym. Sci.* **1977**, *21*, 875.
(5) Roche, E. J.; Pineri, M.; Duplessix, R.; Levelut, A. M. *J. Polym. Sci., Polym. Phys. Ed.* **1981**, *19*, 1.
(6) Litt, M. H. *Polym. Prepr.* **1997**, *38*, 80.
(7) English, A. D.; Vega, A. J. *Macromolecules* **1979**, *12*, 353.
(8) Vega, A. J.; English, A. D. *Macromolecules* **1980**, *13*, 1635.
(9) Brandolini, A. J.; Apple, T. M.; Dybowski, C. *Polymer* **1982**, *23*, 39.
(10) Dec, S. F.; Wind, R. A.; Maciel, G. E. *Macromolecules* **1987**, *20*, 2754.
(11) Isbester, P. K.; Kestner, T. A.; Munson, E. J. *Macromolecules* **1997**, *30*, 2800.
(12) Ando, S.; Harris, R. K.; Hirschinger, J.; Reinsberg, S. A.; Scheler, U. *Macromolecules* **2001**, *34*, 66.
(13) Lehnert, R. J.; Hendra, P. J.; Everall, N.; Clayden, N. J. *Polymer* **1997**, *38*, 1521.

(14) Fontanella, J. J.; Edmondson, C. A.; Wintersgill, M. C.; Wu, Y.; Greenbaum, S. G. *Macromolecules* **1996**, *29*, 4944.
(15) Meresi, G.; Wang, Y.; Bandis, A.; Inglefield, P. T.; Jones, A. A.; Wen, W.-Y. *Polymer* **2001**, *42*, 6153.
(16) Schlick, S.; Gebel, G.; Pineri, M.; Volino, F. *Macromolecules* **1991**, *24*, 3517.
(17) Liu, S.-F.; Schmidt-Rohr, K. *Macromolecules* **2001**, *34*, 8416.
(18) Bennett, A. E.; Rienstra, C. M.; Griffiths, J. M.; Zhen, W.; Lansbury, P. T.; Griffin, R. G. *J. Chem. Phys.* **1998**, *108*, 9463.
(19) Bennett, A. E.; Ok, J. H.; Griffin, R. G.; Vega, S. *J. Chem. Phys.* **1992**, *96*, 8624.
(20) Scheler, U. *Bull. Magn. Reson.* **1999**, *19*, 52.
(21) Su, T.-W.; Tzou, D.-L. M. *Polymer* **2000**, *41*, 7289.
(22) Cobas, J. C.; Sardina, F. J. *Concepts Magn. Reson. A* **2003**, *19A*, 80.
(23) Lesage, A.; Steuernagel, S.; Emsley, L. *J. Am. Chem. Soc.* **1998**, *120*, 7095.
(24) Paddison, S. J.; Thomas, A. Z. *Solid State Ionics* **1998**, *113*−*115*, 333.

MA049759B